Composite Structures 183 (2018) 146–160

Contents lists available at ScienceDirect

Composite Structures

journal homepage: www.elsevier.com/locate/compstruct

Multiobjective optimization of ceramic-metal functionally graded plates using a higher order model

Victor M. Franco Correia [a,b,*], J.F. Aguilar Madeira [a,c], Aurélio L. Araújo [a], Cristóvão M. Mota Soares [a]

[a] IDMEC – Instituto Superior Técnico, Universidade de Lisboa, Av. Rovisco Pais, 1049-001 Lisboa, Portugal
[b] Escola Superior Náutica Infante D. Henrique, Av. Eng. Bonneville Franco, 2770-058 Paço de Arcos, Portugal
[c] Department of Mathematics, ISEL, IPL, Rua Conselheiro Emídio Navarro, 1949-014 Lisboa, Portugal

ARTICLE INFO

Article history:
Received 31 January 2017
Accepted 2 February 2017
Available online 6 February 2017

Keywords:
Multiobjective optimization
Direct MultiSearch
Higher order shear deformation theory
Composites
Functionally graded materials
FGM plates

ABSTRACT

A methodology of multiobjective design optimization of ceramic–metal composite plates with functionally graded materials, with properties varying through the thickness direction, obtained by an adequate variation of volume fractions of the constituent materials, is presented in this paper. Constrained optimization is conducted for different behavior objectives like the maximization of buckling load or fundamental natural frequency. Mass minimization and material cost minimization are also considered. The optimization problems are constrained by stress based failure criteria and other structural response constraints or manufacturing limitations. The design variables are the index of the power-law distribution in the metal-ceramic graded material and the thicknesses of the graded material and/or the metal and ceramic faces.

An equivalent single layer finite element plate model having a displacement field based on a higher order shear deformation theory, accounting for the temperature dependency of the material properties, was developed and validated for the analysis of through-the-thickness ceramic-metal functionally graded plates. The optimization problems are solved with two direct search derivative-free algorithms: GLODS (Global and Local Optimization using Direct Search) and DMS (Direct MultiSearch). DMS, the multiobjective optimization solver, is started from a set of local minimizers which are initially determined by the global optimizer algorithm GLODS for each one of the objective functions.

© 2017 Elsevier Ltd. All rights reserved.

1. Introduction

Functionally graded materials (FGM) are composite materials with a microscopically inhomogeneous character. Continuous changes in their microstructure distinguish FGM from conventional composite materials [1]. The desired mechanical properties of FGM can be obtained in a certain direction through the adequate variation of volume fractions of the constituent materials. The most common FGM are ceramic–metal composites, where the ceramic part has good thermal and corrosion resistance capability and the metallic part provides superior fracture toughness and weldability for example.

In recent years, several plate theories have been used with statics, free vibrations and linear buckling analysis of functionally graded plates. One generic advantage of functionally graded materials (FGM), with properties varying across the thickness direction, when compared to laminated composites, is the continuous variation of material properties that do not present discontinuities across layers.

Recent papers, namely the ones from Jha et al. [2], Swaminathan et al. [3], Thai and Kim [4] and Gupta and Talha [5], have presented extensive reviews on the developed theories for modelling the deformation, stress, vibration and buckling analyses of functionally graded materials and structures, with emphasis to the structural behavior of FGM plates and shells subject to thermo-electro-mechanical loadings under various boundary and environmental conditions. It has been noted [5] that in most of the 2D theories developed to predict the global responses of FGM plates, only the transverse shear deformation effect has been considered and very few theories were found in which both the transverse shear and transverse normal deformation effects were considered. Additionally, it has been noted that the 3D analytical solutions for FGM plates are useful for benchmark purposes, but their solution methods involve mathematical complexities and are difficult and tedious to solve, therefore the use of improved 2D theoretical models which could provide accuracy comparable to the 3D models

* Corresponding author at: Escola Superior Náutica Infante D. Henrique, ENIDH, Av. Eng. Bonneville Franco, 2770-058 Paço de Arcos, Portugal.
E-mail address: victorfranco@enautica.pt (V.M. Franco Correia).

http://dx.doi.org/10.1016/j.compstruct.2017.02.013
0263-8223/© 2017 Elsevier Ltd. All rights reserved.

should be pursued in the interest of computational cost and efficient analyses [2].

According to those review papers it becomes evident that many scientific publications have been devoted to the static analysis, vibration analysis and stability analysis of FGM structures, involving comparisons between different models, but few studies have been dedicated to the design optimization of FGM structures.

Gupta and Talha [5] have also addressed in their review the state of the art in the processing techniques of FGMs, namely the vapor deposition, powder metallurgy, centrifugal casting and solid freeform techniques have been addressed. Previous papers, like the ones from Berger et al. [6], Fukui [7] and Kieback et al. [8] have also addressed the manufacturing techniques of FGMs. Also, Sobczak and Drenchev [9] gave a compact informative review of recent experimental and theoretical activity in the field of functionally graded structures and materials.

Dai et al. [10] have reviewed most of the research done in recent years (2005–2015) on FGM cylindrical structures with an emphasis on coupled mechanics, including thermo-elastic coupling, multiphysic fields coupling, structure–foundation coupling and fluid–solid coupling, and have pointed out possible future directions of research in those areas.

Few works devoted to multiobjective optimization of FGM plate structures, are available in the literature. However, the proper choice of the plate thickness and the functionally graded variation of the metal–ceramic properties across the thickness poses a design issue to be solved aiming to keep the material costs and the structure weight as low as possible while fulfilling certain structural performance for thermo-mechanical loading. The involved design process is multiobjective in nature.

Huang et al. [11] have presented a procedure for bi-objective optimization design of a FGM flywheel by maximizing the kinetic energy and minimizing the maximum Von-Mises stress.

Goupee and Vel [12] have proposed a methodology for the multiobjective optimization of material distribution of functionally graded materials with temperature-dependent material properties for steady thermo-mechanical processes focusing on metal–ceramic and metal–metal functionally graded materials by using a real-coded elitist non-dominated sorting genetic algorithm (NSGA-II). Vel and Pelletier [13] have presented a methodology for the multiobjective optimization of material distribution of functionally graded cylindrical shells for steady thermo-mechanical processes focused on isotropic metal/ceramic and metal/metal FGMs with a material composition assumed to vary in the thickness direction and also using the NSGA-II algorithm.

Among the recently published papers in close relation with the present work, i.e. involving the optimization of FGM structures, but using only single-objective optimization schemes, the following could be mentioned:

Xia and Wang [14] proposed a level set based method for the simultaneous optimization of the material properties and the topology of FG structures with the objective of determining the optimal material properties (via the material volume fractions) and the structural topology to maximize the performance of the structure. Sensitivity analysis was conducted to obtain the descent directions;

Icardi and Ferrero [15] have studied the distributions of properties across the core thickness and in the face sheets of FGM sandwich panels for the minimization of the interlaminar stresses at the interface with the core by solving the Euler–Lagrange equations of a single-objective optimization problem in which the membrane and transverse shear energy contributions are made stationary. In this study, the bending stiffness was maximized while the energy due to interlaminar stresses was minimized;

Na and Kim [16,17] have investigated the volume fraction optimization of FGM panels for stress reduction and improving of thermo-mechanical buckling behavior with the material properties assumed to be temperature dependent and varying continuously in the thickness direction according to a simple power law distribution;

Ashjari and Khoshravan [18] have presented a method for the single-objective optimization of material distribution of simply supported functionally graded plates by using two evolutionary algorithms, namely a genetic algorithm and a particle swarm algorithm;

Taheri and Hassani [19] presented an optimization strategy for eigenfrequency optimization of FG structures within the framework of isogeometric analysis (IGA) approach. The optimization was carried out by using mathematical programming techniques and the required sensitivity analysis was made analytically;

Taheri et al. [20] presented an isogeometrical procedure for optimization of material composition of FG structures in thermo-mechanical processes allowing for gradation of material properties through patches;

Shi and Shimoda [21] have presented an interface shape optimization method for designing FG sandwich structures with two different materials aiming to minimize the compliance of the structure under the volume constraint.

Some other recent related works involving multiobjective optimization studies, not specifically related with FGM structures, but with general fiber reinforced composites, can be mentioned:

Irisarri et al. [22] have presented a multiobjective evolutionary algorithm is presented for stacking sequence optimization of composite structural parts including some design guidelines for stacking sequence design which are included as in the optimization problem as constraints or objectives. The method was applied to the optimal design of a composite plate for weight minimization and maximization of the buckling margins;

Honda et al. [23] have presented a multiobjective optimization approach for fibrous composite plates with curvilinear fibers which uses the non-dominated sorting genetic algorithm (NSGA-II) to obtain the Pareto optimum solutions;

Li and Narita [24] have studied the multiobjective optimal design problem of aeroelastic laminated doubly curved shallow shells where the design objective was the maximization of weighted sum of the critical aerodynamic pressures under different probability density function of flow orientations and the design variable was the fiber orientations in the layers of the symmetrically angle-ply shells.

Within the context of structural design optimization of FGM plate type structures, it is important to adopt sufficiently accurate but also computationally efficient finite element models, based in appropriately selected shear deformation theories, especially when low side-to-thickness ratios are involved, and including the normal strains in the formulation. In the present paper, an equivalent single layer finite element plate model with nine nodes, having a displacement field based on a higher order shear deformation theory with eleven nodal parameters, accounting for the temperature dependency of the material properties, has been developed and validated for the analysis of through-the-thickness ceramic-metal functionally graded plates.

The Direct MultiSearch (DMS) [25] solver for multiobjective optimization problems do not use any derivatives of the objective functions. It is based on a novel technique called direct multisearch, developed by extending direct search from single to multiobjective optimization. The DMS solver has been recently used by Araujo et al. [26] to find the optimal positioning of surface bonded sensors and actuators for damping maximization. It has also been used to solve the problem of minimum weight and maximum damping of a viscoelastic sandwich plates by Madeira et al. [27,28] and to the design optimization of laminated composite plates with piezoelectric layers by Franco Correia et al. [29], among other applications.

In the present paper, the constrained optimization is conducted for different objectives like the maximization of buckling load, maximization of fundamental natural frequency, minimization of mass and minimization of material cost. The multiobjective optimization problems are constrained by stress based failure criteria and other structural response constraints or design/manufacturing limitations. The design variables are the index of the power-law distribution in the metal-ceramic graded material and the thicknesses of the graded material and, if applicable, the metal and ceramic faces.

2. Constitutive relations of the FGM

In the present work it is assumed that the properties of the functionally graded material vary continuously, through the thickness, from a full metal at the bottom of the plate to a full ceramic at the top of the plate, as represented in Fig. 2. The volume fractions of ceramic and metal constituents, V_c and V_m, obtained by the power-law distribution in the metal-ceramic graded material are calculated by [30]

$$V_c = \left(\frac{1}{2} + \frac{z}{h_{tot}}\right)^p, \quad V_m = 1 - V_c \tag{1}$$

where p is the power-law index ($0 \leqslant p \leqslant \infty$) which defines the material variation profile in between the metal-ceramic phase, z is any arbitrary point in the transverse direction and h_{tot} is the total thickness of the plate. Fig. 1 shows the through the thickness variation of the volume fraction V_c with respect to z/h_{tot} for different values of p. The material properties through the thickness are estimated in terms of the individual effective properties of the metal (P_m) and the ceramic (P_c) by the mixture rule (Voigt model [31])

$$P(z) = P_m V_m + P_c V_c. \tag{2}$$

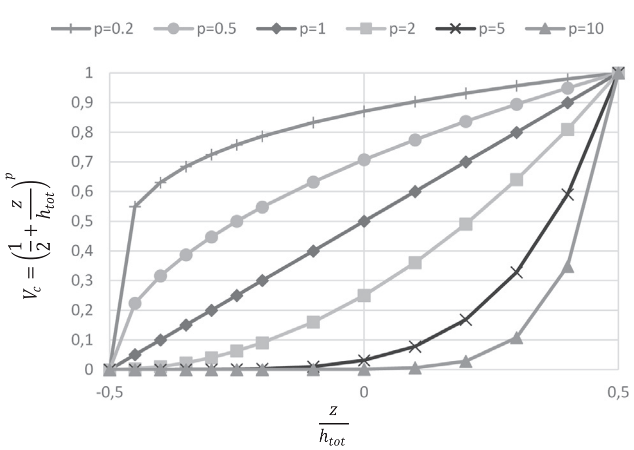

Fig. 1. Through the thickness variation of the volume fraction V_c.

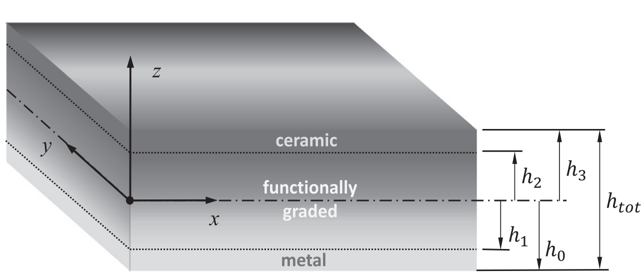

Fig. 2. Geometry definition of the functionally graded metal-ceramic plate.

The material properties, elastic moduli E and G, Poisson coefficient ν, density ρ, thermal coefficient of thermal expansion α, vary according to Eq. (2).

As represented in Fig. 2, a FGM sandwich plate could be defined when a bottom metal skin with non-zero thickness $(h_0 - h_1)$, a top ceramic skin with non-zero thickness $(h_3 - h_2)$ and a FGM intermediate core with thickness of $(h_2 - h_1)$ are considered.

Since functionally graded plate structures are mainly used in high temperature environment and the mechanical properties of the constituent materials suffer significant changes with temperature increase, this temperature-dependency is considered in the present work. The properties can be expressed as a nonlinear function of temperature by the following expression [32]

$$P_f = P_0(P_{-1}T^{-1} + 1 + P_1 T + P_2 T^2 + P_3 T^3) \tag{3}$$

where P_0, P_{-1}, P_1, P_2 and P_3 are the coefficients of the temperature (in Kelvin) given in Table A1 in Appendix [31,32] for some ceramic materials (Zirconium oxide, ZrO_2; Silicon Nitride, Si_3N_4; Aluminum Oxide, Al_2O_3) and for some metals (Stainless steel, SS304; Titanium alloy, Ti-6Al-4V). The temperature (in K) is given by $T = T_0 + \Delta T_0$, where T_0 is the stress free temperature and ΔT_0 is the temperature change.

It is assumed that the variation of temperature occurs in thickness direction only and the temperature is assumed constant in the x-y plane. In this case the temperature distribution along the thickness can be obtained by solving a steady-state heat transfer equation as [33]

$$-\frac{d}{dZ}\left[\kappa(z)\frac{dT}{dZ}\right] = 0 \tag{4}$$

where $\kappa(z)$ is the material thermal conductivity which is variable through the thickness direction and also temperature dependent. By imposing the boundary conditions of $T = T_m$ at $z = -h/2$ and $T = T_c$ at $z = h/2$, the solution of this equation can be obtained [33,34].

The linear constitutive equations, in a generic point in the plate, are given by

$$\boldsymbol{\sigma} = \mathbf{Q}\,\{\boldsymbol{\varepsilon} - \boldsymbol{\varepsilon}^{th}\} \tag{5}$$

$\boldsymbol{\sigma} = \{\sigma_{xx}\ \sigma_{yy}\ \sigma_{zz}\ \sigma_{xy}\ \sigma_{yz}\ \sigma_{xz}\}^T$ is the elastic stress vector, $\boldsymbol{\varepsilon} = \{\varepsilon_{xx}\ \varepsilon_{yy}\ \varepsilon_{zz}\ \gamma_{xy}\ \gamma_{yz}\ \gamma_{xz}\}^T$ is the elastic strain vector and $\boldsymbol{\varepsilon}^{th} = \{1 \quad 1 \quad 1 \quad 0 \quad 0 \quad 0\}^T \alpha(z)\Delta T(z)$ is the thermal vector of strains caused by the temperature change $\Delta T(z) = T(z) - T_0$. T_0 is the stress-free reference temperature, $\alpha(z)$ the coefficient of thermal expansion which varies through the thickness of the plate according to the FGM power-law index and $\mathbf{Q}$ is the elastic constitutive matrix for isotropic materials whose non-zero terms are given explicitly by [35]

$$\begin{aligned} &Q_{11} = \tfrac{E(1-\nu)}{(1+\nu)(1-2\nu)} = Q_{22} = Q_{33}; \quad Q_{12} = \tfrac{E\nu}{(1+\nu)(1-2\nu)} = Q_{13} = Q_{23}; \\ &Q_{44} = \tfrac{1}{2}(Q_{11} - Q_{12}) = Q_{55} = Q_{66} \end{aligned} \tag{6}$$

In order to model the through the thickness variation of material properties of the FGM plate/sandwich, a certain number of virtual layers (NL) with constant thickness are considered, each having the homogeneous material properties calculated by Eqs. (1) and (2). The adequate number of virtual layers has been verified for different values of the exponent p in the power-law in Eq. (1).

3. Finite element model

The displacement components u, v and w at any point in the laminate domain along the x, y and z directions, respectively, are expanded in a Taylor's series powers of the thickness coordinate

Table A1
Temperature-dependent coefficients for some ceramics and metals. *Sources:* Reddy and Chin [32] and Shen and Wang [31], among others.

Materials	Properties	P_0	P_{-1}	P_1	P_2	P_3
Aluminum oxide (Al_2O_3)	E (Pa)	$349.55\times10^{+9}$	0	-3.853×10^{-4}	4.027×10^{-7}	-1.673×10^{-10}
	ν	0.26	0	0	0	0
	ρ (kg/m^3)	3800	0	0	0	0
	α (1/K)	6.8269×10^{-6}	0	1.838×10^{-4}	0	0
	κ (W/m K)	-14.087	-1123.6	-6.227×10^{-3}	0	0
Silicon Nitride (Si_3N_4)	E (Pa)	$348.43\times10^{+9}$	0	-3.070×10^{-4}	2.160×10^{-7}	-8.946×10^{-11}
	ν	0.24	0	0	0	0
	ρ (kg/m^3)	2370	0	0	0	0
	α (1/K)	5.8723×10^{-6}	0	9.095×10^{-4}	0	0
	κ (W/m K)	113.723	0	-1.032×10^{-3}	5.466×10^{-7}	-7.876×10^{-11}
Zirconium oxide (ZrO_2)	E (Pa)	$244.27\times10^{+9}$	0	-1.371×10^{-3}	1.214×10^{-6}	-3.681×10^{-10}
	ν	0.2882	0	1.133×10^{-4}	0	0
	ρ (kg/m^3)	–	0	0	0	0
	α (1/K)	12.766×10^{-6}	0	-1.491×10^{-3}	-1.006×10^{-5}	-6.778×10^{-11}
	κ (W/m K)	1.7	0	1.276×10^{-4}	6.648×10^{-8}	0
Titanium alloy (Ti-66Al-4 V)	E (Pa)	$122.56\times10^{+9}$	0	-4.586×10^{-4}	0	0
	ν	0.2884	0	1.121×10^{-4}	0	0
	ρ (kg/m^3)	4429	0	0	0	0
	α (1/K)	7.5788×10^{-6}	0	6.638×10^{-4}	-3.147×10^{-7}	0
	κ (W/m K)	1.0	0	1.704×10^{-2}	0	0
Stainless steel (SS304)	E (Pa)	$201.04\times10^{+9}$	0	3.079×10^{-4}	-6.534×10^{-7}	0
	ν	0.3262	0	-2.002×10^{-4}	3.797×10^{-7}	0
	ρ (kg/m^3)	8166	0	0	0	0
	α (1/K)	12.330×10^{-6}	0	8.086×10^{-4}	0	0
	κ (W/m K)	15.379	0	-1.264×10^{-3}	2.092×10^{-6}	-7.223×10^{-10}

z. Each component is a function of x, y, z coordinates and time, t. The following higher order displacement field is used [29,36]

$$\begin{aligned} u(x,y,z,t) &= u_0(x,y,t) + z\,\theta_x(x,y,t) + z^2u_0^*(x,y,t) + z^3\phi_x^*(x,y,t)\\ v(x,y,z,t) &= v_0(x,y,t) + z\,\theta_y(x,y,t) + z^2\,v_0^*(x,y,t) + z^3\phi_y^*(x,y,t)\\ w(x,y,z,t) &= w_0(x,y,t) + z\,\phi_z(x,y,t) + z^2w_0^*(x,y,t) \end{aligned} \tag{7}$$

where u_0, v_0, w_0 are the displacements of a generic point on the reference surface, θ_x, θ_y are the rotations of normal to the reference surface about the y and x axes respectively (Fig. 3) and ϕ_z, u_0^*, v_0^*, w_0^*, ϕ_x^*, ϕ_y^* are the higher order terms in the Taylor's series expansions, defined at the reference surface. The present finite element model based on the above displacement field has nine nodes and eleven unknowns at each node: u_0, v_0, w_0, θ_x, θ_y, ϕ_z, u_0^*, v_0^*, w_0^*, ϕ_x^*, ϕ_y^* and will be referred to as HSDT11. For this displacement field the elastic strains are given by

$$\begin{Bmatrix} \varepsilon_{xx}\\ \varepsilon_{yy}\\ \varepsilon_{zz}\\ \gamma_{xy}\\ \gamma_{yz}\\ \gamma_{xz} \end{Bmatrix} = \begin{Bmatrix} \frac{\partial u_0}{\partial x}\\ \frac{\partial v_0}{\partial y}\\ \phi_z\\ \frac{\partial u_0}{\partial y}+\frac{\partial v_0}{\partial x}\\ \theta_y+\frac{\partial w_0}{\partial y}\\ \theta_x+\frac{\partial w_0}{\partial x} \end{Bmatrix} + z\begin{Bmatrix} \frac{\partial \theta_x}{\partial x}\\ \frac{\partial \theta_y}{\partial y}\\ 2\,w_0^*\\ \frac{\partial \theta_x}{\partial y}+\frac{\partial \theta_y}{\partial x}\\ 2v_0^*+\frac{\partial \phi_z}{\partial y}\\ 2u_0^*+\frac{\partial \phi_z}{\partial x} \end{Bmatrix} + z^2\begin{Bmatrix} \frac{\partial u_0^*}{\partial x}\\ \frac{\partial v_0^*}{\partial y}\\ 0\\ \frac{\partial u_0^*}{\partial y}+\frac{\partial v_0^*}{\partial x}\\ 3\phi_y^*+\frac{\partial w_0^*}{\partial y}\\ 3\phi_x^*+\frac{\partial w_0^*}{\partial x} \end{Bmatrix} + z^3\begin{Bmatrix} \frac{\partial \phi_x^*}{\partial x}\\ \frac{\partial \phi_y^*}{\partial y}\\ 0\\ \frac{\partial \phi_x^*}{\partial y}+\frac{\partial \phi_y^*}{\partial x}\\ 0\\ 0 \end{Bmatrix}. \tag{8}$$

By applying the Hamilton's principle to obtain the finite element equilibrium equations, neglecting the damping effects, it can be written

$$\delta\int_{t_1}^{t_2}\left\{\int_A\left(\dot{\mathbf{u}}^T\left(\int_z\rho\,dz\right)\dot{\mathbf{u}} - \int_z\boldsymbol{\varepsilon}^T\boldsymbol{\sigma}\;dz\;+\;p\,w\right)dA\right\}\,dt\;=\;0 \tag{9}$$

where $\mathbf{u}$ represents the generalized displacements, i.e. $\mathbf{u} = \{u, v, w\}$, $\dot{\mathbf{u}} = \frac{\partial\mathbf{u}}{\partial t}$, V and A represent, respectively, the volume and area of the representative material domain under consideration, $\boldsymbol{\varepsilon}$ are the strains and $\boldsymbol{\sigma}$ the stresses in an arbitrary point of the domain and $p(x,y)$ are the transversal forces applied to the plate. After integration, it becomes

$$\int_{t_1}^{t_2}\left\{\int_A\left(\delta\,\dot{\mathbf{u}}^T\left[\int_z\;\rho\,dz\right]\ddot{\mathbf{u}} + \int_z[\delta\,\boldsymbol{\varepsilon}^T\boldsymbol{\sigma}]\,dz\;-\;p\,\delta w\right)dA\right\}\,dt\;=\;0. \tag{10}$$

By applying the Hamilton's principle to obtain the finite element equilibrium equations, neglecting the damping effects, it can be written

$$\delta\int_{t_1}^{t_2}\left\{\int_A\left(\dot{\mathbf{u}}^T\left(\int_z\rho\,dz\right)\dot{\mathbf{u}} - \int_z\boldsymbol{\varepsilon}^T\boldsymbol{\sigma}\;dz\;+\;p\,w\right)dA\right\}\,dt\;=\;0 \tag{11}$$

where $\mathbf{u}$ represents the generalized displacements, i.e. $\mathbf{u} = \{u, v, w\}$, $\dot{\mathbf{u}} = \frac{\partial\mathbf{u}}{\partial t}$, V and A represent, respectively, the volume and area of the representative material domain under consideration, $\boldsymbol{\varepsilon}$ are the strains and $\boldsymbol{\sigma}$ the stresses in an arbitrary point of the domain and $p(x,y)$ are the transversal forces applied to the plate. After integration, it becomes

$$\int_{t_1}^{t_2}\left\{\int_A\left(\delta\,\dot{\mathbf{u}}^T\left[\int_z\;\rho\,dz\right]\ddot{\mathbf{u}} + \int_z\;[\,\delta\,\boldsymbol{\varepsilon}^T\boldsymbol{\sigma}\,]\,dz\;-\;p\,\delta w\right)dA\right\}\,dt\;=\;0. \tag{12}$$

Considering, that $\boldsymbol{\sigma} = \mathbf{Q}\,\{\boldsymbol{\varepsilon} - \boldsymbol{\varepsilon}^{th}\}$, if the plate domain is divided in a finite number of element domains, with area A_e, the previous equation can be written as

$$\int_{t_1}^{t_2}\left\{\sum_{e=1}^{NE}\int_{A_e}\left(\delta\,\mathbf{u}^{eT}\left(\int_z\;\rho\,dz\right)\ddot{\mathbf{u}}^e + \int_z[\delta\,\boldsymbol{\varepsilon}^{eT}\mathbf{Q}^e\,(\boldsymbol{\varepsilon}^e - \boldsymbol{\varepsilon}^{eth})]\,dz\right.\right.$$
$$\left.\left.-\;p^e\,\delta w\right)dA\right\}dt\;=\;0 \tag{13}$$

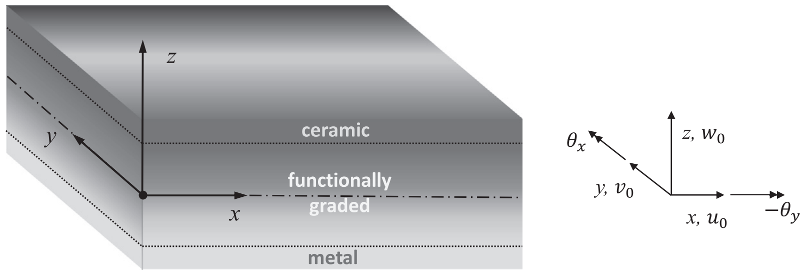

Fig. 3. Displacements and rotations definition in the FGM metal-ceramic plate.

where NE is the number of finite elements in the domain and the superscript e is referred to the element. In the context of the finite element implementation it can be written

$$\int_{t_1}^{t_2}\left\{\sum_{e=1}^{NE}\int_{A_e}\left(\delta\mathbf{q}^{eT}\,\mathbf{N}^T\left(\int_z\rho\,dz\right)\mathbf{N}\ddot{\mathbf{q}}^e+\int_z\left[\delta\mathbf{q}^{eT}\,\mathbf{B}^T\mathbf{Z}^T\mathbf{Q}\,\mathbf{Z}\mathbf{B}\,\mathbf{q}^e - \delta\mathbf{q}^{eT}\mathbf{B}^T\mathbf{Z}^T\mathbf{Q}\,\boldsymbol{\varepsilon}^{eth}\right]dz - \delta\mathbf{q}^{eT}\mathbf{F}^e\right)dA\right\}dt = 0 \tag{14}$$

where $\mathbf{N}$ are the shape functions for the nine-node plate finite element and $\mathbf{B}$ is the strain displacements matrix [36]. Furthermore, the functional can be written as

$$\int_{t_1}^{t_2}\left\{\sum_{e=1}^{NE}\left(\delta\mathbf{q}^{eT}\,\mathbf{M}^e\,\ddot{\mathbf{q}}^e+\delta\mathbf{q}^{eT}\,\mathbf{K}^e\,\mathbf{q}^e - \delta\mathbf{q}^{eT}\mathbf{F}^{eth} - \delta\mathbf{q}^{eT}\,\mathbf{F}^e\right)\right\}dt = 0 \tag{15}$$

where $\mathbf{K}^e$ and $\mathbf{M}^e$ are, respectively the element stiffness and mass matrices, generically obtained by

$$\mathbf{K}^e = \int_{-1}^{+1}\int_{-1}^{+1}\mathbf{B}^T\left(\sum_{k=1}^{NL}\int_{h_{k-1}}^{h_k}\mathbf{Z}^T\ \mathbf{Q}_k\ \mathbf{Z}\ dz\right)\ \mathbf{B}\ det\mathbf{J}\ d\xi\ d\eta \tag{16}$$

$$\mathbf{M}^e = \int_{-1}^{+1}\int_{-1}^{+1}\mathbf{N}^T\left(\sum_{k=1}^{NL}\rho_k\int_{h_{k-1}}^{h_k}\mathbf{Z}_m^T\ \mathbf{Z}_m\ dz\right)\ \mathbf{N}\ det\mathbf{J}\ d\xi\ d\eta \tag{17}$$

being $\mathbf{Z}$ and $\mathbf{Z}_m$ matrices of powers of the z coordinate which are defined in accordance with the displacement field [37], $\mathbf{q}^e$ is the nodal displacements vector for an arbitrary element and $\mathbf{F}^{eth}$ is the thermal component, calculated as

$$\mathbf{F}^{eth} = \int_{A_e}\int_z\mathbf{B}^T\mathbf{Q}^e\,\boldsymbol{\varepsilon}^{eth}\,dz\,dA = \int_{-1}^{+1}\int_{-1}^{+1}\mathbf{B}^T\left(\sum_{k=1}^{NL}\int_{h_{k-1}}^{h_k}\mathbf{Z}^T\mathbf{Q}_k\begin{Bmatrix}\alpha_k\Delta T_k\\ \alpha_k\Delta T_k\\ \alpha_k\Delta T_k\\ 0\\ 0\\ 0\end{Bmatrix}dz\right)det\mathbf{J}\ d\xi\ d\eta. \tag{18}$$

The coordinates ξ,η are the standard natural coordinates with the origin defined at the center of the element, and the element is defined from −1 to +1. Details related with the calculation of matrices $\mathbf{B}$ and $\mathbf{Z}$ for the present higher order displacement field could be obtained from previous works [29,36] among other resources.

Assuming arbitrary variations of $\delta\mathbf{q}^e$ and adding the element matrices, according to the element topology, in the standard way, one obtains the system equilibrium equation

$$\mathbf{M}\ddot{\mathbf{q}}+\mathbf{K}\ \mathbf{q} = \mathbf{F}+\mathbf{F}^{th}. \tag{19}$$

For linear static type problems one obtains the general equilibrium equation,

$$\mathbf{K}\ \mathbf{q} = \mathbf{F}+\mathbf{F}^{th} \tag{20}$$

where $\mathbf{F}^{th}$ is the thermal vector, which represents the fictitious forces modelling thermal expansion.

For free vibrations, considering the vibration mode n, the eigenvalue problem

$$(\mathbf{K} - \omega_n^2\ \mathbf{M})\ \mathbf{q}_n = 0 \tag{21}$$

can be obtained, where ω_n represents the natural frequency of the plate for mode n and $\mathbf{q}_n$ is the corresponding eigenmode.

If one considers the initial stresses, by applying the Hamilton's principle to the appropriate Lagrangean functional, for an arbitrary finite element e in the domain, and adding the contribution of all the elements in the domain, the global equilibrium equation can be written as

$$(\mathbf{K} + \mathbf{K}_\sigma)\ \mathbf{q} + \mathbf{M}\ \ddot{\mathbf{q}} = \mathbf{F}+\mathbf{F}^{th} \tag{22}$$

where $\mathbf{K}_\sigma$ is the geometric stiffness matrix. From this equation, it results the linear elastic buckling standard eigenvalue problem

$$\mathbf{K}\ \mathbf{q} + \lambda\ \mathbf{K}_\sigma\ \mathbf{q} = 0 \tag{23}$$

where λ represents the buckling parameter. The geometric stiffness matrix is generically obtained by for an arbitrary element in the domain, as [37]

$$\mathbf{K}_\sigma^e = \int_{-1}^{+1}\int_{-1}^{+1}\mathbf{B}_G^T\left(\sum_{k=1}^{NL}\int_{h_{k-1}}^{h_k}\mathbf{Z}_G^T\begin{bmatrix}\sigma_k^0 & 0 & 0\\ 0 & \sigma_k^0 & 0\\ 0 & 0 & \sigma_k^0\end{bmatrix}\mathbf{Z}_G\ dz\right)\times\mathbf{B}_G\ det\mathbf{J}\ d\xi\ d\eta \tag{24}$$

where the initial stresses matrix σ_k^0, for a generic virtual FGM lamina k, is defined as

$$\sigma_k^0 = \begin{bmatrix}\sigma_{xx}^0 & \sigma_{xy}^0 & \sigma_{xz}^0\\ \sigma_{xy}^0 & \sigma_{yy}^0 & \sigma_{yz}^0\\ \sigma_{xz}^0 & \sigma_{yz}^0 & \sigma_{zz}^0\end{bmatrix}_k \tag{25}$$

and $\mathbf{B}_G$ is a strain-displacement matrix containing the shape functions and its derivatives in accordance with the displacement field and $\mathbf{Z}_G$ is a matrix containing powers of the z coordinate and verifying the relation [37]

$$\left\{\frac{\partial u}{\partial x},\frac{\partial u}{\partial y},\frac{\partial u}{\partial z},\frac{\partial v}{\partial x},\frac{\partial v}{\partial y},\frac{\partial v}{\partial z},\frac{\partial w}{\partial x},\frac{\partial w}{\partial y},\frac{\partial w}{\partial z}\right\}^T = \mathbf{Z}_G\left\{\frac{\partial u_0}{\partial x},\frac{\partial u_0}{\partial y},\theta_x,\frac{\partial v_0}{\partial x},\frac{\partial v_0}{\partial y},\theta_y,\frac{\partial w_0}{\partial x},\frac{\partial w_0}{\partial y},\phi_z^*,\frac{\partial\theta_x}{\partial x},\frac{\partial\theta_x}{\partial y},\right.$$
$$2u_0^*,\frac{\partial\theta_y}{\partial x},\frac{\partial\theta_y}{\partial y},2v_0^*,\frac{\partial\phi_z^*}{\partial x},\frac{\partial\phi_z^*}{\partial y},2w_0^*,\frac{\partial u_0^*}{\partial x},\frac{\partial u_0^*}{\partial y},3\phi_x^*,\frac{\partial v_0^*}{\partial x},\frac{\partial v_0^*}{\partial y},$$
$$\left.3\phi_y^*,\frac{\partial w_0^*}{\partial x},\frac{\partial w_0^*}{\partial y},\frac{\partial\phi_x^*}{\partial x},\frac{\partial\phi_x^*}{\partial y},\frac{\partial\phi_y^*}{\partial x},\frac{\partial\phi_y^*}{\partial y}\right\}^T = \mathbf{Z}_G\ \mathbf{B}_G\ \mathbf{q}^e\ . \tag{26}$$

4. Multiobjective optimization

In the present work, the following strategy is used to solve the multiobjective optimization (MOO) problem:

1) First, the local extremes for each one of the objectives are determined. It means that if the multiobjective problem has k objectives, then k single-objective optimization problems are solved with a global optimization program. This task is performed with the Global and Local Optimization using Direct Search (GLODS) algorithm [38] for single optimization, suited for bound constrained, derivative-free and global optimization.
2) Secondly, the multiobjective optimization algorithm is initialized with all local extremes obtained in the previous steps. This task is solved with the Direct MultiSearch (DMS) method [25].

This strategy is used considering that, if the objectives are contradictory the MOO problem has a set of optimal solutions instead of a single solution. In addition, the optimal solution of each single-objective problem, when the objective functions are considered separately, is part of the set of optimal solutions of multiobjective problem.

A general structural multiobjective optimization problem can be formulated as [25,39,40]:

Find n design variables

$$\mathbf{x} = (x_1,\ x_2,\ \dots\ ,\ x_n)^T \in \Omega \subseteq IR^n, \tag{27}$$

which minimize:

$$\min_{\mathbf{x}\in\Omega} F(\mathbf{x}) \equiv (f_1(\mathbf{x}), f_2(\mathbf{x}), \dots, f_k(\mathbf{x}))^T, \tag{28}$$

involving $k > 1$ objective functions or objective function components $f_i : \Omega \subseteq IR^n \to IR \cup \{+\infty\}, i = 1, \dots, k$ and being Ω a feasible region.

The feasible region Ω can be defined by inequality constraints like

$$g_{l_1}(\mathbf{x}) \leqslant 0, \quad l_1 = \{1, 2, \dots, m_1\} \tag{29}$$

and bound constraints imposed in the design variables, as

$$x_i^l \leqslant x_i \leqslant x_i^u, \quad i = 1, \dots, n \tag{30}$$

where x_i^l and x_i^u are respectively, the lower and upper limits of the design variables.

In the presence of several objective functions, the set of design variables, which minimize one function, are not necessarily the same, which minimize another function. To define some sort of optimality, it is crucial to establish a way for comparing different solutions, such as the concept of Pareto dominance:

Given two points $\mathbf{x}, \mathbf{y} \in \Omega$, it can be said that $\mathbf{x} \prec \mathbf{y}$ ($\mathbf{x}$ dominates $\mathbf{y}$) if and only if $f_i(\mathbf{y}) \leqslant f_i(\mathbf{x})$ for all $i = \{1, 2, \dots, k\}$ with $f_j(\mathbf{y}) < f_j(\mathbf{x})$ for at least one $j, j \in \{1, 2, \dots, k\}$.

A set of points in Ω is non-dominated when no point in the set is dominated by another one in the set. The concept of Pareto dominance is thus used to characterize optimality in multiobjective optimization, by defining the set of Pareto optimizers or non-dominated points.

More formally, a point $\mathbf{x}^* \in \Omega$ is said to be a (global) Pareto optimizer or a non-dominated point of F in Ω if there is no $\mathbf{y} \in \Omega$ such that $\mathbf{y} \prec \mathbf{x}^*$. The Pareto frontier or efficient frontier is the mapping by F of such set of Pareto optimizers.

Direct MultiSearch (DMS) [25] is a derivative-free method for multiobjective optimization problems, which does not aggregate any components of the objective function. It is inspired by the search/poll paradigm of direct-search methods of directional type, extended from single to multiobjective optimization and uses the concept of Pareto dominance to maintain a list of feasible non-dominated points. The new feasible points evaluated in each iteration are added to this list and the dominated ones are removed. Successful iterations correspond then to changes in the list, meaning that a new feasible non-dominated point was found. Otherwise, the iteration is declared as unsuccessful.

In the DMS method, the constraints are handled using an extreme barrier function

$$f_\Omega(\mathbf{x}) = \begin{cases} f(\mathbf{x}) & \textit{if } \mathbf{x} \in \Omega \\ (+\infty, \dots, +\infty) & \textit{otherwise} \end{cases} \tag{31}$$

When a point is unfeasible, the components of the objective function F are not evaluated, and the values of $\boldsymbol{F}_\Omega$ are set to $+\infty$. This approach allows dealing with black-box type constraints, where only a yes/no type of answer is returned. Details are omitted in the present paper and the reader is referred to Custodio et al. [25] for a more complete description of this method.

In this paper, two different processes are used to select the non-dominated solutions:(i) All non-dominated solutions can be projected in the planes $f_i - f_j$, with i ranging from 1 to the number of objective functions and j ranging from i +1 to the number of objective functions and the non-dominated solutions which stand out from these projections are analysed;(ii) The objective functions can be normalized and the identification of the best solutions N_1, N_2 and N_∞ for the norms L_1, L_2 and L_∞, respectively, defined as

$$L_1 = \min\left(\sum_{i=1}^{n} A_{i,1}, \sum_{i=1}^{n} A_{i,2}, \dots, \sum_{i=1}^{n} A_{i,k}\right) \tag{32}$$

$$L_2 = \min\left[\left(\sum_{i=1}^{n} (A_{i,1})^2\right)^{1/2}, \left(\sum_{i=1}^{n} (A_{i,2})^2\right)^{1/2}, \dots, \left(\sum_{i=1}^{n} (A_{i,k})^2\right)^{1/2}\right] \tag{33}$$

$$L_\infty = \min(\max{}_{i=1,\dots,n} A_{i,1}, \max{}_{i=1,\dots,n} A_{i,2}, \dots, \max{}_{i=1,\dots,n} A_{i,k}) \tag{34}$$

where $A_{i,j}$ is the normalized matrix of non-dominated solutions, where i $(i = 1, \dots, n)$ represents the objective functions and j ranges from 1 to k, where k which represents the number of non-dominated solutions. If A is the matrix of the non-dominated solutions, the normalized matrix $A_{i,j}$ is calculated by

$$A_{i,j} = \frac{A_{i,j} - \min{}_j A_{i,j}}{\max{}_j A_{i,j} - \min{}_j A_{i,j}}. \tag{35}$$

The norms L_1, L_2 and L_∞, and the solutions N_1, N_2 and N_∞, can be evaluated for all n objective functions or, alternatively, just for some of the objective functions depending on certain design interests. This subject will be shown in detail in one numerical example.

5. Numerical applications

5.1. Validation of FGM model for statics, free vibration and linear buckling problems

For validation purposes of the FGM model, the first numerical study is a simply supported square, $a \times a$, FGM plate, where the metal constituent is Aluminum and the ceramic constituent is Alumina, Al_2O_3, with a side-to-thickness ratio of $a/h = 10$. The non-dimensional transversal deflection, at $(x, y) = (\frac{a}{2}, \frac{a}{2})$, caused by a uniform load q_0 is calculated for several power indexes p and compared with the exact solutions of Zenkour [41] and also from Thai and Choi [42] and Bui et al. [43] in Table 1. The present solution, referred to as HSDT11, has been obtained with an 8×8 finite element mesh for the full plate representation.

Table 1
Non-dimensional transversal deflection, $w = \frac{10h^3 E_c}{a^4 q_0} w(\frac{a}{2}, \frac{a}{2})$ of simply supported FGM Al/ Al_2O_3 square plate subjected to uniform transversal load.

	p index								
	Ceramic	1	2	3	5	7	9	10	Metal
HSDT11	0.46422	0.92149	1.1796	1.3034	1.4212	1.4939	1.5536	1.5808	2.5201
Zenkour[41]	0.4665	0.9287	1.1940	1.3200	1.4356	1.5049	1.5617	1.5876	2.5327
Thai and Choi [42]	0.4666	0.9288	1.1909	1.3123	1.4205	1.4867	1.5433	1.5697	2.5329
Bui et al. [43]	0.4630	0.9130	1.2069	1.3596	1.4874	–	–	1.6308	2.5120

The non-dimensional deflection is given by $w = \frac{10h^3 E_c}{a^4 q_0} w(\frac{a}{2}, \frac{a}{2})$. The material properties considered for the Aluminum are: E_m = 70 GPa, ν = 0.3, ρ = 2702 kg/m^3 and for the ceramic Al_2O_3: E_c = 380 GPa, ν = 0.3, ρ = 3800 kg/m^3.

In Fig. 4 it is shown the convergence of the non-dimensional deflection with respect to the number of virtual layers along the thickness of the FGM plate for index p = 1.

Table 2 shows the non-dimensional stress components calculated in the indicated points in the simply supported square plate subjected to the uniform load q_0 for several values of power p. Here, the stresses for the homogeneous full metal and full ceramic are equal as expected.

The fundamental natural frequencies of a simply supported square FGM plate, where the metal constituent is Aluminum and the ceramic constituent is Zirconia, ZrO_2, are presented and compared with alternative results in Table 3. The assumed material properties for the ceramic are, E_c = 200 GPa, ν = 0.3, ρ = 5700 kg/m^3.

Table 3
Non-dimensional fundamental natural frequencies, $\omega' = \omega h \sqrt{\rho_c / E_c}$, of the simply supported FGM Al/ZrO_2 square plate.

	$p = 1$ $a/h = 10$	$p = 1$ $a/h = 20$	$p = 2$ $a/h = 5$	$p = 5$ $a/h = 5$
HSDT11	0.0597	0.0158	0.2118	0.2126
Qian et al. [44]	0.0596	0.0153	0.2153	0.2194
Neves et al. [45]	0.0596	0.0153	0.2198	0.2225
Neves et al. [46]	0.0596	0.0153	0.2201	0.2230

The temperature change effect on a FGM Silicon Nitride as ceramic and Stainless Steel as metal, Si_3N_4/SS304, simply supported plate is validated in Table 4 and compared with recently published results from Bui et al. [43]. A rectangular plate with $a/b = 0.3333$ and a square plate, $a/b = 1$, are considered. The plate with a side-to-thickness ratio of $a/h = 10$, is subjected to a transversal uniform load q_0 and $p = 1$ also to the effect of a global temperature

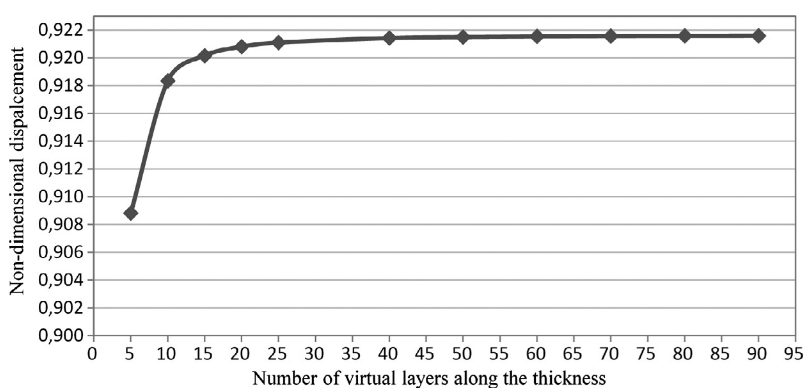

Fig. 4. Convergence of non-dimensional deflection with respect to the number of virtual layers along the thickness of the FGM Al/Al_2O_3 plate (p = 1).

Table 2
Non-dimensional stresses in the simply supported square FGM Al/Al_2O_3 plate subjected to an uniform load q_0.

	p index						
	Ceramic	1	2	5	7	10	Metal
	$\sigma'_{xx}(\frac{a}{2}, \frac{a}{2}, \frac{h}{2}) = \frac{h}{q_0 a} \sigma_{xx}(\frac{a}{2}, \frac{a}{2}, \frac{h}{2})$						
HSDT11	2.923	4.500	5.216	6.008	6.405	6.927	2.923
Zenkour [41]	2.8932	4.4745	5.2296	6.1504	6.6547	7.3689	2.8932
	$\sigma'_{yy}(\frac{a}{2}, \frac{a}{2}, \frac{h}{3}) = \frac{h}{q_0 a} \sigma_{yy}(\frac{a}{2}, \frac{a}{2}, \frac{h}{3})$						
HSDT11	1.929	2.194	2.053	1.624	1.460	1.296	1.929
Zenkour [41]	1.9103	2.1692	2.0338	1.6104	1.4467	1.2820	1.9103
	$\sigma'_{zz}(\frac{a}{2}, \frac{a}{2}, \frac{h}{2}) = \frac{h}{q_0 a} \sigma_{zz}(\frac{a}{2}, \frac{a}{2}, \frac{h}{2})$						
HSDT11	0.1247	0.1540	0.1804	0.2395	0.2632	0.2869	0.1247
	$\tau'_{xy}(0, 0, \frac{h}{2}) = \frac{h}{q_0 a} \tau_{xy}(0, 0, \frac{h}{2})$						
HSDT11	-1.329	-2.532	-3.235	-3.811	-3.916	-4.015	-1.329
	$\tau'_{yz}(\frac{a}{2}, 0, 0) = \frac{h}{q_0 a} \tau_{yz}(\frac{a}{2}, 0, 0)$						
HSDT11	0.5886	0.6421	0.6074	0.5077	0.5077	0.5233	0.5886
	$\tau'_{xz}(0, \frac{a}{2}, 0) = \frac{h}{q_0 a} \tau_{xz}(0, \frac{a}{2}, 0)$						
HSDT11	0.5868	0.6385	0.6039	0.5043	0.5041	0.5196	0.5868

Table 4
Non-dimensional center deflection, $w' = \frac{100wE_mh^3}{12(1-\nu_m^2)q_0a^4}$, of a simply supported $a \times b$, FGM Si_3N_4/SS304 plate subjected to a uniform transversal load and a global temperature change ($p = 1$).

Temperature (K)	300	400	500	600	700	800
$a/b = 1$						
HSDT11	0.1196	0218	0.1247	0.1282	0.1325	0.1380
Bui et al. [43]	0.1219	0.1242	0.1270	0.1306	0.1353	0.1412
$a/b = 0.3333$						
HSDT11	0.2366	0.2408	0.2461	0.2527	0.2609	0.2712
Bui et al. [43]	0.2364	0.2407	0.2462	0.2533	0.2624	0.2739

increase from 300 K to 800 K in 100 K steps. The non-dimensional center deflections calculated by

$$w' = \frac{100wE_mh^3}{12(1-\nu_m^2)q_0a^4}$$

are presented in Table 4 and compared in Fig. 5, for a power index. An excellent agreement with the alternative solution has been obtained.

In Table 5 it is shown the non-dimensional deflections for the situation where the metal side of the FGM plate is kept at a constant temperature of 300 K (stress free temperature) and the temperature on the ceramic side is increased from 300 K to 800 K. Table 5 and Fig. 6 show the non-dimensional deflections for three different power index values: $p = 1, p = 0.2$ and $p = 10$.

The buckling load calculation is compared in Table 6 with the alternative results published by Lafiti et al. [47] obtained for simply supported thin rectangular functionally graded plates by using the classical Plate Theory and Fourier series expansion for several power law indexes. In this numerical example, the constituent materials are Alumina, Al_2O_3, as ceramic and Aluminum as metal. The Alumina properties are $E_c = 380$ GPa, $\nu_c = 0.3$. Here the Aluminum properties are: $E_m = 70$ GPa, $\nu_m = 0.3$. No temperature variation has been considered. A uniaxial distributed load N_x is considered. The total plate thickness is $h = 0.5$ mm and the length along y-axis is $b = 0.5$ m ($b/h = 1000$). A better agreement is found for the aspect ratio $b/a = 1$ than for $b/a = 2$.

In Table 7, the buckling loads for thick rectangular functionally graded plates are compared with alternative values. One is alternative values published by Thai and Choi [48] which have been obtained by a refined theory accounting for a quadratic variation of the transverse shear strains across the thickness and satisfying the zero traction boundary conditions on the top and bottom surfaces of the plate. Another alternative solution is the one obtained by Bodaghi and Saidi [49] based on a Levy-type higher-order deformation plate theory. In this example, the constituent materials are Silicon Carbide as ceramic, again with Aluminum as metal. The Silicon Carbide (SiC) properties are $E_c = 4200$ GPa, $\nu_c = 0.3$. Once more, a uniaxial distributed load N_x is considered. A few length-to-thickness b/h ratios ($b = 1$ m) and power law indexes are considered and a good agreement has been found.

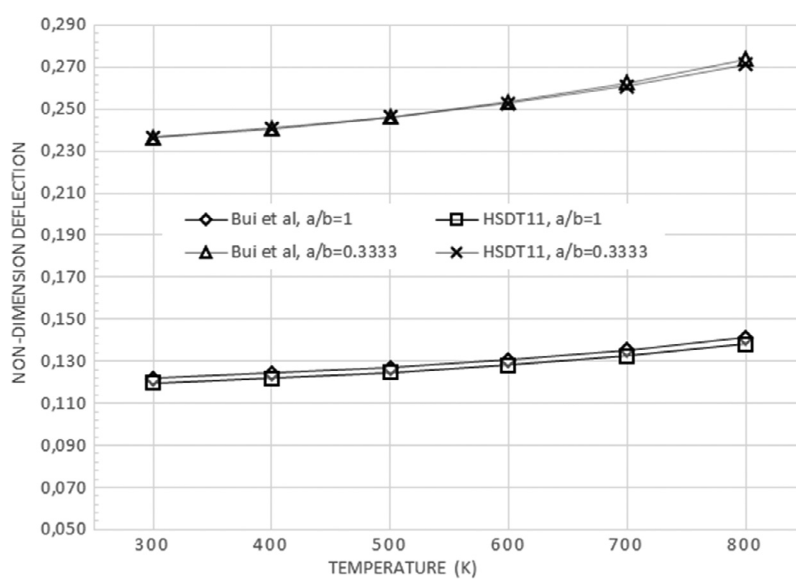

Fig. 5. Comparison of central deflections of a simply supported $a \times b$, FGM Si_3N_4/SS304 plate subjected to a uniform transversal load and a temperature change.

Table 5
Non-dimensional center deflection, $w' = \frac{100wE_mh}{12(1-\nu^2)q_0a^4}$, of a simply supported $a/b = 1$, FGM Si_3N_4/SS304 plate subjected to a uniform transversal pressure q_0 and a temperature change on the ceramic side with the metal side temperature constant at 300 K.

Temperature at ceramic side (K)	300	400	500	600	700	800
HSDT11 $p = 1$	0.1196	0.1206	0.1215	0.1225	0.1234	0.1244
HSDT11 $p = 0.2$	0.1059	0.1069	0.1078	0.1086	0.1094	0.1101
HSDT11 $p = 10.$	0.1367	0.1375	0.1385	0.1397	0.1413	0.1432

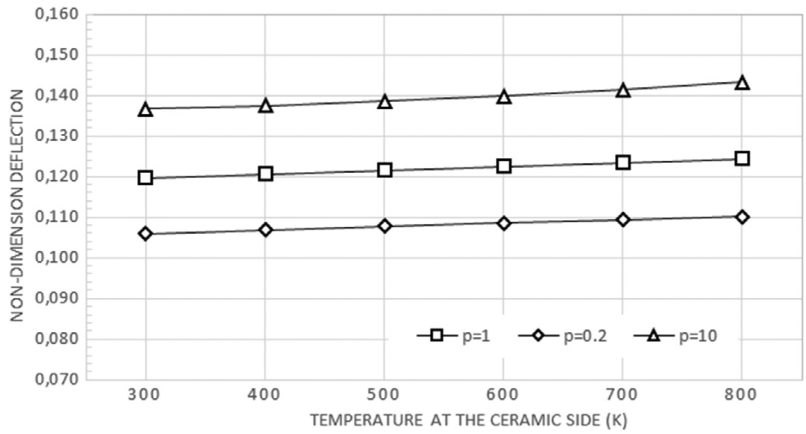

Fig. 6. Central deflections of a simply supported $a/b = 1$, FGM Si_3N_4/SS304 plate subjected to a uniform transversal load and a temperature change on the ceramic side (temperature at metal side 300 K).

Table 6
Buckling load N_x ($\times 10^5$ N) comparison for thin FGM (Al/Al_2O_3) simply supported rectangular plates for several values of the power law index.

	b/a	$p = 0$	$p = 1$	$p = 2$	$p = 5$
HSDT11	1	6.7859	3.3844	2.6386	2.2283
	2	9.7282	4.8574	3.7872	3.1938
Lafiti el al [47] CPT Fourier expansion	1	6.811	3.392	2.650	2.241
	2	10.630	5.312	4.130	3.512

Table 7
Buckling load N_x ($\times 10^6$ N) comparison for thick FGM (Al/SiC) simply supported rectangular plates for different values of the power law indexes.

	b/a	b/h	$p = 0$	$p = 1$	$p = 2$
HSDT11	0.5	10	2120.25	1056.27	803.689
	1	10	1446.84	717.445	551.473
	1	5	9761.66	4906.33	3720.82
Thai & Choi [48], Refined theory	0.5	10	2079.758	1028.449	780.023
	1	10	1437.389	702.251	534.835
	1	5	9916.193	4955.484	3746.732
Bodaghi and Saidi[49], Levy-type high-order theory	0.5	10	2079.721	1028.412	780.097
	1	10	1437.361	702.304	534.441
	1	5	9915.620	4955.431	3746.054

5.2. Multiobjective optimization of FGM plates

The multiobjective optimization of an FGM simply supported plate ($a \times b$) is now considered with a few illustrative design optimization cases. The FGM plate ($a = b = 0.5$ m) is subjected to a uniform in-plane compression load of $N_x = 1000$ N and a uniformly distributed transverse loading of 10^5 N/m^2, causing bending compressive stresses on the metal side and tensile bending stresses on the ceramic side. An FGM material combination with Silicon Nitride as ceramic and Stainless Steel as metal (Si_3N_4/SS304) is considered.

Three design optimization cases are considered with identical objective functions (f_1,f_2,f_3,f_4), as follows:

i. (f_1) maximization of the fundamental natural frequency, with desired frequencies falling in the range: $3000\ \text{rad/s} \leqslant \omega_1 \leqslant 8000\ \text{rad/s}$;
ii. (f_2) maximization of the buckling load parameter, with the design goal: $\lambda \geqslant 1$;
iii. (f_3) minimization of the overall mass of the plate;
iv. (f_4) minimization of the total material cost of the plate.

All solutions not fulfilling the conditions established for objective functions f_1 and f_2 are rejected. In all cases the temperature is kept constant at 300 K, either at ceramic and at metal side. The material properties are the ones from Table A1 given in Appendix. Stress based failure criteria (Tsai-Hill) are imposed in the ceramic, metal and graded phases. The isotropic tensile and compressive strengths, X_T and X_C, respectively, and the shear strength, S, are given in Table 8.

The three design optimization cases are distinguished by the design variables which have been considered:

1. In the first case, two design variables are considered:
   i. the power law index, p, assuming: $0.2 \leqslant p \leqslant 10$, as represented in Fig. 1 (with possible increments of 0.1);
   ii. the total thickness of the FGM graded material.

The FGM thickness has a lower bound of 5 mm and a upper bound of 60 mm, with possible increments of 0.1 mm.

Table 8
Material strengths in tension, compression and shear (MPa).

	X_T	X_C	S
Silicon Nitride (Si_3N_4)	360	689	207.8
Stainless Steel (SS304)	215	215	124

2. In the second case, the power law index is fixed as $p = 1$ and three design variables are considered as follows:
   i. the thickness of the metal skin, with a lower bound of zero and an upper bound of 60 mm, with possible increments of 0.1 mm;
   ii. the total thickness of the FGM graded material, with a lower bound of 5 mm and a upper bound of 60 mm, with possible increments of 0.1 mm;
   iii. the thickness of the ceramic skin, with a lower bound of zero and an upper bound of 60 mm, with possible increments of 0.1 mm;
3. In the third case, four design variables are considered as follows:
   i. the power law index, p, assuming: $0.2 \leqslant p \leqslant 10$ (with possible increments of 0.1);
   ii. the thickness of the metal skin, with a lower bound of zero and an upper bound of 60 mm, with possible increments of 0.1 mm;
   iii. the total thickness of the FGM graded material, with a lower bound of 5 mm and a upper bound of 60 mm, with possible increments of 0.1 mm;
   iv. the thickness of the ceramic skin, with a lower bound of zero and an upper bound of 60 mm, with possible increments of 0.1 mm;

In the first design optimization case, only one block of graded material has been considered. In the other two design optimization cases, and depending on the solutions obtained for the design variables thicknesses, it can be obtained one full metal face and/or one full ceramic face and it always exists one FGM graded core in between those faces. The total thickness of the plate cannot exceed the imposed upper bound of 60 mm.

The solutions N_1, N_2 and N_∞ which are, from all non-dominated normalized solutions, the best solutions for norms L_1 (Eq. (30)), L_2 (Eq. (31)) and L_∞ (Eq. (32)), respectively, have been calculated considering all objective functions (f_1, f_2, f_3, f_4) or just some of those objective functions, depending on design requirements. Those norms are presented in Tables 9, 10 and 11, respectively for the three design optimization cases which have been considered. Additionally, the non-dominated solutions which minimize or maximize the individual objective functions, which have been designated by $S_i$with,$i = 1 \ldots 4$, are also presented with the best individual objective functions.

The projections of all non-dominated solutions, respectively, for the first, second and third design optimization cases, are represented in Fig. 7, 8 and 9, using six representative plots, namely: (i) the minimization of mass versus the minimization of the material cost; (ii) the maximization of buckling load parameter versus the maximization of fundamental natural frequency; (iii) the maximization of the fundamental natural frequency versus the minimization of mass $(f_1 - f_3)$; (iv) the maximization of buckling load parameter versus the minimization of mass $(f_2 - f_3)$; (v) the maximization of the fundamental natural frequency versus the minimization of the material cost $(f_1 - f_4)$; (vi) and the maximization of buckling load parameter versus the minimization of the material cost $(f_2 - f_4)$.

Noting that the Young modulus of the ceramic Si_3N_4 is higher than the one of SS304 stainless steel and the density is much lower, an higher percentage of ceramic material would lead to higher plate stiffness and also a lower mass, for the same comparative thickness. The material cost for the SS304 stainless steel is assumed to be 3 USD/kg and the material cost for the Silicon Nitride (Si_3N_4) is assumed to be 50 USD/kg, based on average market values obtained for the representative material from some international suppliers. In this case, the minimization of material cost is an objective function which is conflicting with the mass minimization.

Table 9, shows the solutions S_1, S_2, S_3, S_4 which minimize the single objective functions f_1, f_2, f_3, f_4, respectively, obtained by GLODS algorithm [30], for the first design optimization case where

Table 9
Results for the first design optimization case having four design objectives (f_1, f_2, f_3, f_4) and two design variables (power law index p and total thickness of the FGM material) for the FGM plate Si_3N_4/SS304.

Solutions	*Objective functions*				*Design variables*	
	1st natural frequency (rad/s)	Buckling load parameter (n.d.)	Mass (kg)	Material cost (USD)	p	Thicknessof the FGM ($\times 10^{-3}$ m)
Initial design	5760.81	1.298	46.10	1022.96	1	35.0
S_1	**8000.00**	2.845	101.20	1076.50	3.4	59.1
S_2	7987.20	**2.867**	105.11	1012.87	4	60.0
S_3	5705.86	1.004	**21.50**	872.99	0.2	25.8
S_4	4629.91	1.004	68.76	**403.79**	10	36.0
$N_1(f_1,f_2)$	7993.51	2.867	104.58	1023.27	3.9	59.9
N_2 (f_1,f_2), $N_\infty(f_1,f_2)$ $N_\infty(f_1,f_2)$	7996.15	2.859	103.30	1043.59	3.7	59.6
$N_1(f_1,f_3)$	7982.20	1.965	30.34	1231.66	0.2	36.4
$N_2(f_1,f_3)$	61.01	1.954	30.25	1228.28	0.2	36.3
$N_\infty(f_1,f_3)$	7770.00	1.862	29.50	1197.82	0.2	35.4
$N_1(f_1,f_4)$	7478.13	2.619	114.60	672.99	10	60.0
$N_2(f_1,f_4)$	7364.96	2.540	112.69	661.77	10	59.0
$N_\infty(f_1,f_4)$	6930.26	2.249	105.43	619.15	10	55.2
$N_1(f_2,f_3)$	7982.20	1.965	30.34	1231.66	0.2	36.4
$N_2(f_2,f_3)$	7995.75	2.179	41.45	1390.12	0.4	41.2
$N_\infty(f_2,f_3)$	7986.41	2.250	46.24	1425.75	0.5	43.0
$N_1(f_2,f_4)$	6821.33	2.060	83.81	925.47	3.2	49.4
$N_2(f_2,f_4)$	7342.27	2.524	112.31	659.53	10	58.8
$N_\infty(f_2,f_4)$	6884.08	2.219	104.67	614.66	10	54.8
$N_1(f_3,f_4)$	4622.81	1.000	68.48	405.94	9.8	35.9
$N_2(f_3,f_4)$	4718.51	1.001	60.09	579.02	4	34.3
$N_\infty(f_3,f_4)$	4841.09	1.009	53.20	721.22	2.3	33.2
N_1 (f_2,f_3,f_4),N_2 (f_2,f_3,f_4)	7982.20	1.965	30.34	1231.66	0.2	36.4
N_∞ (f_2,f_3,f_4)	6534.60	1.839	72.75	986.25	2.3	45.4
N_1 (f_1,f_2,f_3,f_4),N_2 (f_1,f_2,f_3,f_4)	7982.20	1.965	30.34	1231.66	0.2	36.4
N_∞ $(f_1,f_2,f_3,f_4.)$	6534.60	1.839	72.75	986.25	2.3	45.4

Table 10
Results for the second design optimization case having four design objectives (f_1, f_2, f_3, f_4) and three design variables (thickness of the 100% metal, thickness of the FGM graded material, thickness of the 100% ceramic) for the FGM plate Si_3N_4/SS304. The power law index is fixed with $p = 1$.

Solutions	*Objective functions*				*Design variables*
	1st natural frequency (rad/s)	Buckling load parameter (n.d.)	Mass (kg)	Material cost (USD)	Thicknesses (metal + FGM + ceramic) ($\times 10^{-3}$ m)
Initial design	5753.58	1.299	46.10	978.90	0.5 + 25.0 + 0.5 = 35.0
S_1	**7999.98**	2.294	46.85	1128.13	4.0 + 13.9 + 25.9 = 43.8
S_2	7999.39	**2.924**	106.20	673.35	48.0 + 5.1 + 6.8 = 59.9
S_3	5629.07	1.001	**22.139**	701.07	0 + 5.0 + 21.3 = 26.3
S_4	4776.63	1.011	54.526	**469.56**	23.0 + 5.0 + 5.0 = 33.0
$N_1(f_1,f_2)$, $N_2(f_1,f_2)$, $N_\infty(f_1,f_2)$	7999.95	2.824	92.306	800.54	39.0 + 6.3 + 11.2 = 56.5
$N_1(f_1,f_3)$	7989.23	1.932	27.95	972.84	0 + 5.0 + 30.8 = 35.8
$N_2(f_1,f_3)$	7964.72	1.876	27.65	958.42	0 + 5.0 + 30.3 = 35.3
$N_\infty(f_1,f_3)$	7565.86	1.744	26.92	923.85	0 + 5.0 + 29.1 = 34.1
$N_1(f_1,f_4)$	7870.00	2.858	108.91	624.83	50.0 + 5.0 + 5.0 = 60.0
$N_2(f_1,f_4)$	7763.22	2.778	106.88	618.99	49.0 + 5.0 + 5.0 = 59.0
$N_\infty(f_1,f_4)$	7439.28	2.545	100.80	601.51	46.0 + 5.0 + 5.0 = 56.0
$N_1(f_2,f_3)$	7998.60	2.027	31.91	1002.79	2.0 + 5.2 + 30.6 = 37.8
$N_2(f_2,f_3)$	7998.88	2.260	44.21	1042.35	9.0 + 5.4 + 28.6 = 43.0
$N_\infty(f_2,f_3)$	7994.16	2.325	48.44	1050.99	11.0 + 6.2 + 27.3 = 44.5
$N_1(f_2,f_4)$	7870.00	2.858	108.91	624.83	50.0 + 5.0 + 5.0 = 60.0
$N_2(f_2,f_4)$	6887.47	2.170	90.69	572.51	41.0 + 5.0 + 5.0 = 51.0
$N_\infty(f_2,f_4)$	6681.08	2.036	86.72	564.13	39.0 + 5.0 + 5.1 = 49.1
$N_1(f_3,f_4)$	4776.63	1.011	54.53	469.56	23.0 + 5.0 + 5.0 = 33.0
$N_2(f_3,f_4)$	4885.60	1.001	46.06	568.50	17.0 + 5.0 + 9.5 = 31.5
$N_\infty(f_3,f_4)$	4983.27	1.006	41.97	615.64	14.0 + 5.0 + 11.9 = 30.9
$N_1(f_2,f_3,f_4)$	7870.00	2.858	108.91	624.83	50.0 + 5.0 + 5.0 = 60.0
$N_2(f_2,f_3,f_4)$	6945.60	2.075	72.12	741.13	29.0 + 5.0 + 12.8 = 46.8
$N_\infty(f_2,f_3,f_4)$	6904.92	1.987	64.21	794.22	24.0 + 5.0 + 15.7 = 44.7
$N_1(f_1,f_2,f_3,f_4)$	7989.23	1.932	27.95	972.84	0 + 5.0 + 30.8 = 35.8
$N_2(f_1,f_2,f_3,f_4)$	7987.67	2.123	36.83	1023.46	5.0 + 5.0 + 30.0 = 40.0
$N_\infty(f_1,f_2,f_3,f_4)$	7170.87	2.080	60.49	865.24	21.0 + 5.0 + 18.9 = 44.9

Table 11
Results for the third design optimization case having four design objectives (f_1, f_2, f_3, f_4) and four design variables (power law index p, thickness of the 100% metal face, thickness of the FGM graded material, thickness of the 100% ceramic face) for the FGM plate Si_3N_4/SS304.

Solutions	*Objective functions*				*Design variables*	
	1st natural frequency (rad/s)	Buckling load parameter (n.d.)	Mass (kg)	Material cost (USD)	p	Thicknesses (metal + FGM + ceramic) ($\times 10^{-3}$ m)
Initial design	5753.58	1.299	46.10	978.90	1	0.5 + 25.0 + 0.5 = 35.0
S_1	**8000.00**	2.845	101.20	1076.50	3.4	0 + 59.1 + 0 = 59.1
S_2	7993.58	**2.927**	106.77	632.38	0.2	49.0 + 5.0 + 6.0 = 60.0
S_3	6046.18	1.033	**17.680**	772.082	0.2	0 + 5.0 + 20.0 = 25.0
S_4	4701.21	1.026	64.315	**335.074**	0.2	30.0 + 5.0 + 0 = 35.0
$N_1(f_1,f_2)$, $N_2(f_1,f_2)$, $N_\infty(f_1,f_2)$	7999.73	2.913	104.60	678.53	9.6	8.0 + 40.5 + 11.0 = 59.5
$N_1(f_1,f_3)$, $N_2(f_1,f_3)$	7992.22	1.853	25.37	1079.13	0.2	0 + 10.2 + 24.0 = 34.2
$N_\infty(f_1,f_3)$	7841.83	1.7777	24.60	1050.23	0.2	0 + 9.4 + 24.0 = 33.4
$N_1(f_1,f_4)$, $N_2(f_1,f_4)$	7662.54	2.746	112.46	535.34	0.2	53.0 + 5.0 + 2.0 = 60.0
$N_\infty(f_1,f_4)$	7275.06	2.483	107.83	495.91	0.2	51.0 + 5.1 + 1.0 = 57.1
$N_1(f_2,f_3)$	7995.60	2.084	34.46	982.05	1.8	1.0 + 7.0 + 31.0 = 39.0
$N_2(f_2,f_3)$	7995.50	2.248	43.12	989.28	2.2	4.0 + 8.6 + 30.0 = 42.6
$N_\infty(f_2,f_3)$	7984.19	2.305	47.05	996.11	2	7.0 + 8.0 + 29.0 = 44.0
$N_1(f_2,f_4)$, $N_2(f_2,f_4)$	7268.86	2.494	111.23	474.66	0.2	53.0 + 5.0 + 0.0 = 58.0
$N_\infty(f_2,f_4)$	6841.09	2.205	103.07	450.30	0.2	49.0 + 5.0 + 0.0 = 54.0
$N_1(f_3,f_4)$	5483.35	1.010	25.51	661.32	8.9	1.0 + 5.4 + 21.0 = 27.4
$N_2(f_3,f_4)$	4985.62	1.004	40.73	540.16	9.4	9.0 + 6.6 + 15.0 = 30.6
$N_\infty(f_3,f_4)$	4995.15	1.006	40.59	549.07	4.8	9.0 + 6.6 + 15.0 = 30.6
$N_1(f_2,f_3,f_4)$	7993.58	2.927	106.77	632.38	0.2	49.0 + 5.0 + 6.0 = 60.0
$N_2(f_2,f_3,f_4)$	7091.63	2.135	69.43	711.34	10	23.0 + 5.8 + 18.0 = 46.8
$N_\infty(f_2,f_3,f_4)$	6901.49	1.983	63.08	720.42	8.6	3.0 + 22.4 + 19.0 = 44.4
$N_1(f_1,f_2,f_3,f_4)$	7992.19	2.696	77.33	818.99	9.6	9.0 + 22.8 + 21.0 = 52.8
$N_2(f_1,f_2,f_3,f_4)$	7994.11	2.362	50.05	957.73	10	4.0 + 12.1 + 29.0 = 45.1
$N_\infty(f_1,f_2,f_3,f_4)$	7273.87	2.110	57.72	813.89	9.3	5.0 + 16.6 + 23.0 = 44.6

the design variables are the thickness of the FGM material and the power law $N_1(f_3,f_4)$ index p. The best multiobjective optimization solutions, obtained with DMS algorithm [25], for the three different norms which have been evaluated considering the objective functions $(f_i, f_j, \ldots)$ are represented as $N_1(f_i, f_j, \ldots)$, $N_2(f_i, f_j, \ldots)$ and $N_\infty(f_i, f_j, \ldots)$. The solutions $N_i(f_1, f_2, f_3, f_4), i = 1, 2, \infty$, represent the best design compromise, of the FGM thickness and index p, considering all objective functions. If these solutions are

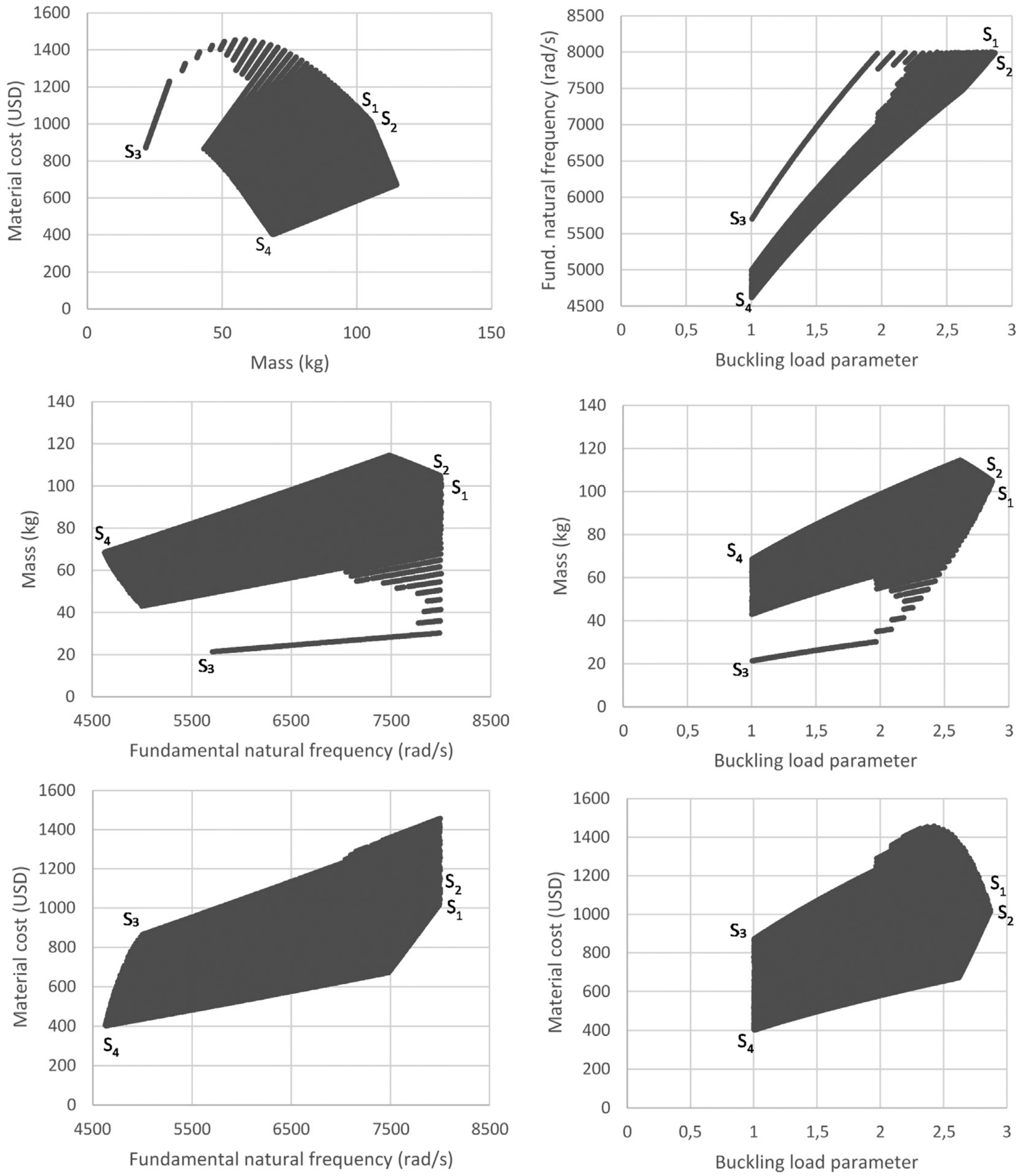

Fig. 7. Projection of all non-dominated solutions for the first design optimization case, having two design variables (power law index p and the total thickness of the FGM material), which have been represented in six representative plans.

compared, for example, with the solutions $N_i(f_3,f_4), i = 1, 2, \infty$, worst performance is obtained in what respects the fundamental natural frequency and buckling load parameter, but it can be noted better solutions for the objective of minimum mass in solution $N_1(f_3,f_4)$ and/or better solutions for the objective minimum material cost. The solutions $N_i(f_1,f_2), i = 1, 2, \infty$ lead to the best design compromise considering the fundamental natural frequency and buckling load parameter, but worst performance in objectives f_3 and f_4, ie. mass and material cost.

If the design concern is mainly the minimum mass and minimum material cost, provided that the first natural frequency and buckling load parameter values are inside de bounds initially established, one can chose the solutions $N_1(f_3,f_4)$, $N_2(f_3,f_4)$ or $N_\infty(f_3,f_4)$, calculated with the norms considering only the objective functions of interest, f_3 and f_4, ie. the mass and material cost. If the minimum mass and minimum material cost are a concern but it is also important to maximize the buckling load parameter, one can chose the solutions $N_1(f_2,f_3,f_4)$, $N_2(f_2,f_3,f_4)$ or $N_\infty(f_2,f_3,f_4)$, calculated with the objective functions of interest, f_2, f_3 and f_4.

In Fig. 7, are represented the projections of the non-dominated solutions for the first design optimization cases in six different plans, which are useful to locate the Pareto-front set, including the plots of mass and the material cost $(f_3 - f_4)$, the buckling load parameter and the fundamental natural frequency $(f_1 - f_2)$, the fundamental natural frequency and the mass $(f_1 - f_3)$, the buckling load parameter and the mass $(f_2 - f_3)$, the fundamental natural frequency and the material cost $(f_1 - f_4)$ and the buckling load parameter and material cost $(f_2 - f_4)$. The solutions S_1, S_2, S_3 and S_4 are represented on those plots in order to improve the analysis.

Table 10, shows the solutions for the second design optimization case where the design variables are the thickness of the metal face, thickness of the FGM core material and the thickness of the

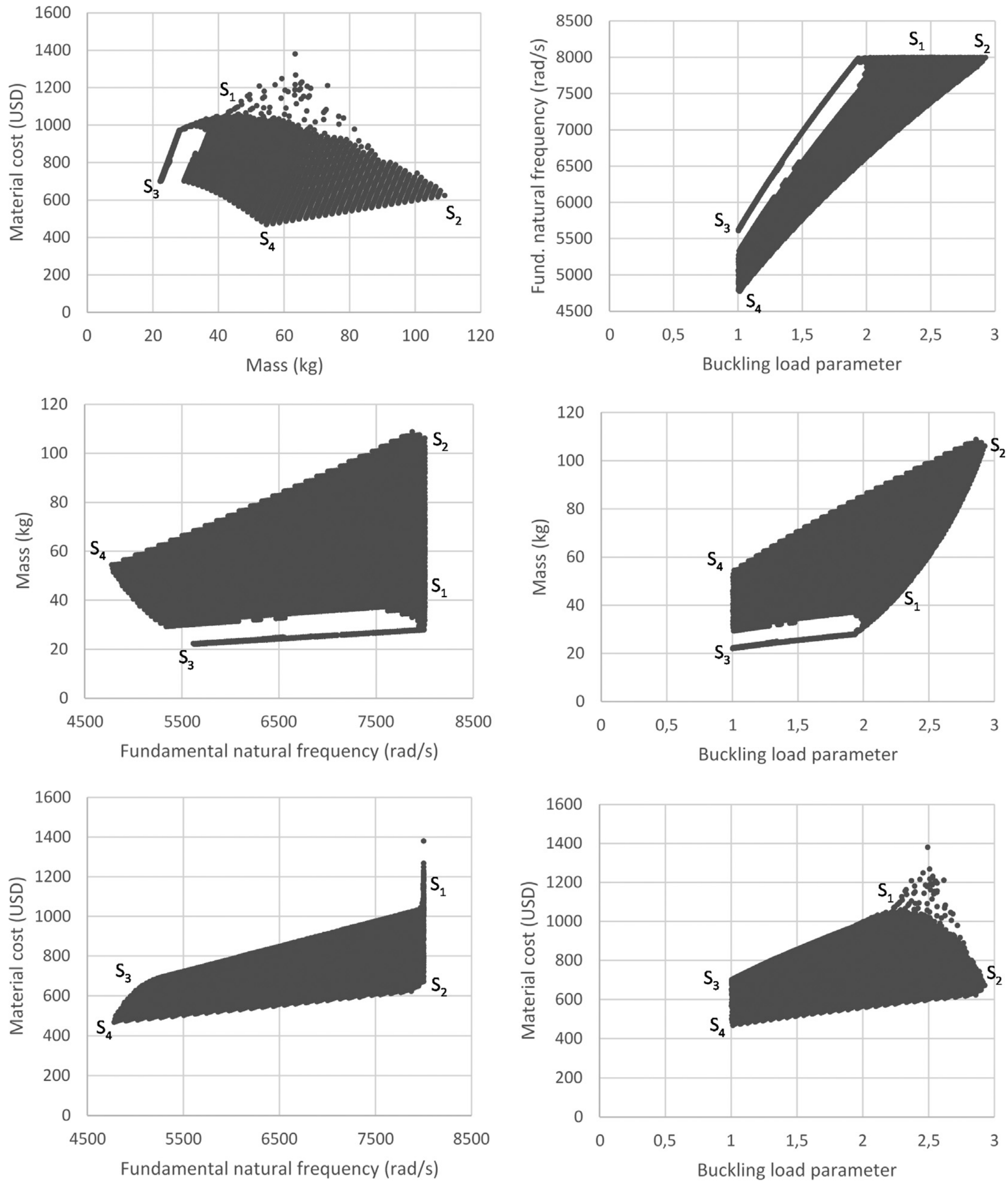

Fig. 8. Projection of all non-dominated solutions for the second design optimization case, having three design variables (thickness of the 100% metal, thickness of the FGM graded material, thickness of the 100% ceramic), which have been represented in six representative plans.

ceramic face, fixing the power law index as $p = 1$. The best multiobjective optimization solutions, obtained with DMS algorithm, for the three different norms which have been evaluated considering the objective functions $(f_i, f_j, \ldots)$ are represented as $N_1(f_i, f_j, \ldots)$, $N_2(f_i, f_j, \ldots)$ and $N_\infty(f_i, f_j, \ldots)$. The solutions $N_i(f_1, f_2, f_3, f_4), i = 1, 2, \infty$, represent the best design compromise, of the three thickness values, considering all objective functions. Solutions with higher thickness in the ceramic face do improve the objective minimization of mass, for similar performance in the maximization of fundamental natural frequency and maximization of buckling load parameter, but the objective of minimization of material cost is worst. Solutions with higher thickness in the metal face tend to present worst performance in the objective of minimization of mass but do present better results in the objective of minimization of material cost.

In Fig. 8, are represented the projections of the non-dominated solutions for the second design optimization case in six different plans, as explained before. Again, the solutions S_1, S_2, S_3 and S_4 are represented on those plots.

Finally, Table 11, shows the solutions for the third design optimization case where the design variables are the thickness of the metal face, thickness of the FGM core material, thickness of the ceramic face and the power law index p. The best multiobjective optimization solutions, obtained with DMS algorithm, for the three different norms which have been evaluated considering the objective functions $(f_i, f_j, \ldots)$ are also represented as $N_1(f_i, f_j, \ldots)$, $N_2(f_i, f_j, \ldots)$ and $N_\infty(f_i, f_j, \ldots)$. The solutions $N_i(f_1, f_2, f_3, f_4), i = 1, 2, \infty$, represent the best design compromise, of the three thickness values and the index p, considering all objective functions. If the design emphasis is attributed to the mass and

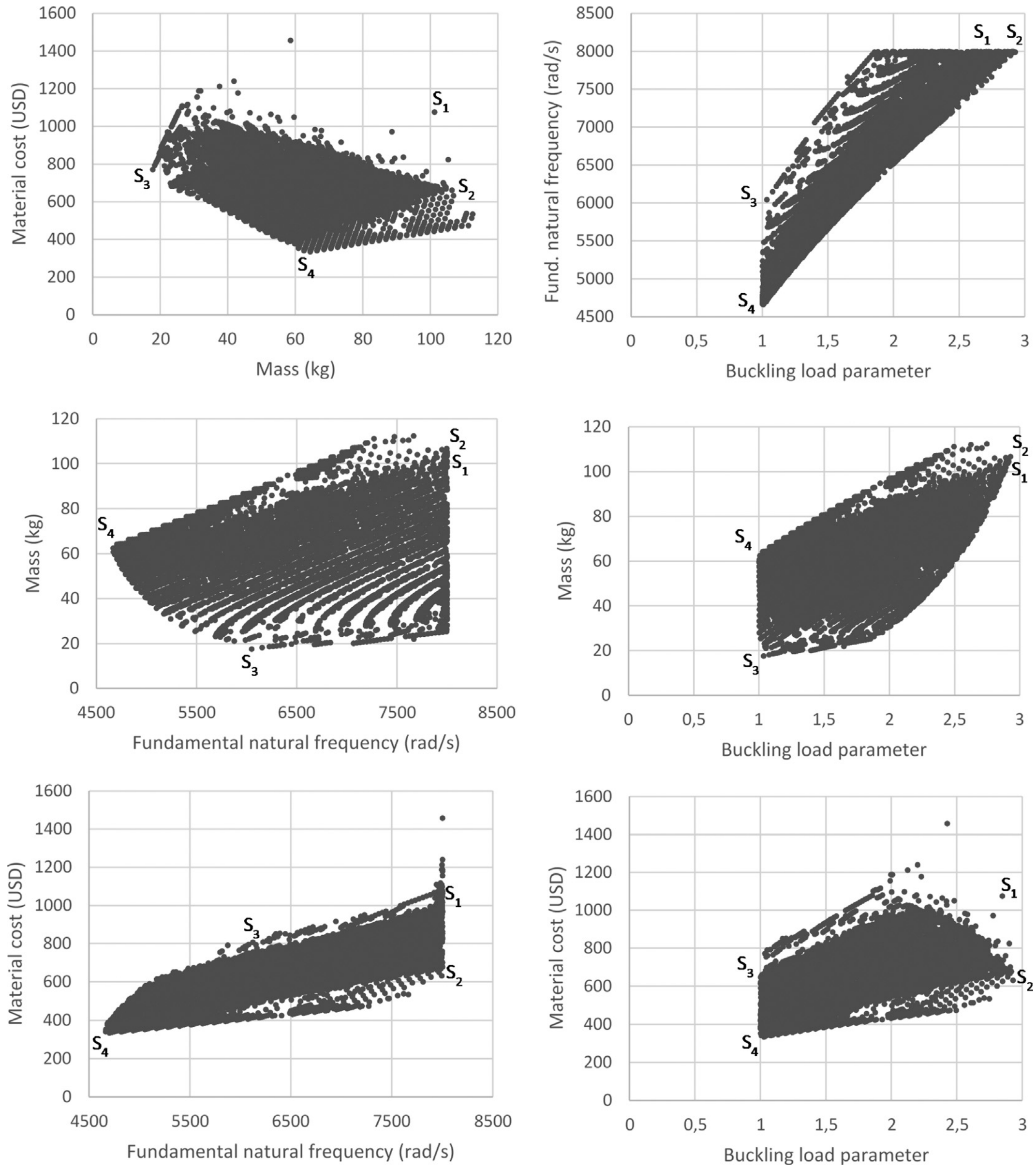

Fig. 9. Projection of all non-dominated solutions for the third design optimization case, having four design variables (power law index p, thickness of the metal face, thickness of the FGM graded material and thickness of the ceramic face), which have been represented in six representative plans.

material cost, while fulfilling the performance minimums established for the fundamental natural frequency and buckling load parameter, the solutions $N_i(f_3, f_4), i = 1, 2, \infty$, lead to better solutions in what concerns to the objectives f_3 and f_4, ie. minimum mass and minimum material cost, respectively.

Finally, in Fig. 9, are represented the projections of the non-dominated solutions for the third design optimization case in six different plans, as for the previous cases, and the solutions S_1, S_2, S_3 and S_4 are also represented on those plots.

6. Conclusions

The development of a mathematical model to describe the static, dynamic and linear buckling behavior of through-the-thickness functionally graded material plate structures has been presented in this paper. The application of the theory has been illustrated through benchmark cases reported in the literature. A good correlation has been obtained between the developed finite element model, which is based in a higher order shear deformation plate theory, and several alternative solutions recently published by other authors. The temperature dependency of the material properties of the FGM has been considered in the model formulation.

In order to maximize the performance of the FGM plate structures in the design process of such structures, the developed finite element model has been associated with a multiobjective optimization technique that has been implemented in connection with two direct search derivative-free algorithms: GLODS (Global and Local Optimization using Direct Search) and DMS (Direct Multi Search).

The illustrative design optimization cases with conflicting objectives, have demonstrated the use of the present multiobjective optimization tool applied to the optimal design of metal-ceramic functionally graded material plates, showing that considerable savings in mass and material cost can be attained and emphasizing the compromises which can be established between those savings and the improvement of structural behavior, namely considering the maximization of the fundamental natural frequency and/or the maximization of the buckling load parameter.

Acknowledgments

This work is dedicated in honor of Professor Yoshihiro Narita on his 65th birthday for his contribution and impact to Research and Education on Mechanics of Advanced Materials and Structures, Computational Mechanics and Engineering Optimization.

This work was supported by FCT, *Fundação para a Ciência e Tecnologia*, through IDMEC - LAETA, project UID/EMS/50022/2013.

References

[1] Koizumi M. FGM activities in Japan. Compos B 1997;28B:1–4.
[2] Jha DK, Kant T, Singh RK. A critical review of recent research on functionally graded plates. Compos Struct 2013;96:833–49.
[3] Swaminathan K, Naveenkumar DT, Zenkour AM, Carrera E. Stress, vibration and buckling analyses of FGM plates – a state-of-the-art review. Compos Struct 2015;120:10–31.
[4] Thai HT, Kim SE. A review of theories for the modeling and analysis of functionally graded plates and shells. Compos Struct 2015;128:70–86.
[5] Gupta A, Talha M. Recent development in modeling and analysis of functionally graded materials and structures. Prog Aerosp Sci 2015. http://dx.doi.org/10.1016/j.paerosci.2015.07.001i.
[6] Berger R, Kwon P, Dharan CKH [High speed centrifugal casting of metal matrix composites]. In: The Fifth International Symposium on Transport Phenomena and Dynamics of Rotating Machinery, Maui, Hawaii, May 8-11.
[7] Fukui Y. Fundamental investigation of functionally gradient materials manufacturing system using centrifugal force. JSME Int. J. Ser. 1991;III (34):144–8.
[8] Kieback B, Neubrand A, Riedel H. Processing techniques for functionally graded materials. Mater Sci Eng, A 2003;362:81–105.
[9] Sobczak JJ, Drenchev L. Metallic functionally graded materials: a specific class of advanced composites. J. Mater. Sci. Technol. 2013;29–4:297–316.
[10] Dai HL, Rao YN, Dai T. A review of recent researches on FGM cylindrical structures under coupled physical interactions, 2000–2015. Compos Struct 2016;152:199–225.
[11] Huang J, Fadel GM, Blouin VY, Grujicic M. Bi-objective optimization design of functionally gradient materials. Mater Des 2002;23:657–66.
[12] Goupee AJ, Vel SS. Multi-objective optimization of functionally graded materials with temperature-dependent material properties. Mater Des 2007;28:1861–79.
[13] Vel SS, Pelletier JL. Multi-objective optimization of functionally graded thick shells for thermal loading. Compos Struct 2007;81:386–400.
[14] Xia Q, Wang MY. Simultaneous optimization of the material properties and the topology of functionally graded structures. Comput Aided Des 2008;40:660–75.
[15] Icardi U, Ferrero L. Optimization of sandwich panels with functionally graded core and faces. Compos Sci Technol 2009;69(5):575–85.
[16] Na KS, Kim JH. Optimization of volume fractions for functionally graded panels considering stress and critical temperature. Compos Struct 2009;89:509–16.
[17] Na KS, Kim JH. Volume fraction optimization for step-formed functionally graded plates considering stress and critical temperature. Compos Struct 2010;92:1283–90.
[18] Ashjari M, Khoshravan MR. Mass optimization of functionally graded plate for mechanical loading in the presence of deflection and stress constraints. Compos Struct 2014;110:118–32.
[19] Taheri AH, Hassani B. Simultaneous isogeometrical shape and material design of functionally graded structures for optimal eigenfrequencies. Comput Methods Appl Mech Eng 2014;277:46–80.
[20] Taheri AH, Hassani B, Moghaddam NZ. Thermo-elastic optimization of material distribution of functionally graded structures by an isogeometrical approach. Int J Solids Struct 2014;51:416–29.
[21] Shi JX, Shimoda M. Interface shape optimization of designing functionally graded sandwich structures. Compos Struct 2015;125:88–95.
[22] Irisarri FX, Bassir DH, Carrere N, Maire JF. Multiobjective stacking sequence optimization for laminated composite structures. Compos Sci Technol 2009;69:983–90.
[23] Honda S, Igarashi T. Narita, Y. Multi-objective optimization of curvilinear fiber shapes for laminated composite plates by using NSGA-II, Composites: Part B 2013;45:1071–8.
[24] Li J, Narita Y. Multi-objective design for aeroelastic flutter of laminated shallow shells under variable flow angles. Compos Struct 2014;111:530–9.
[25] Custodio AL, Madeira JFA, Vaz AIF, Vicente LN. Direct Multisearch for Multiobjective Optimization. SIAM J Optim 2011;21(3):1109–40.
[26] Araújo AL, Madeira JFA, Mota Soares CM, Mota Soares CA. Optimal design for active damping in sandwich structures using the Direct MultiSearch Method. Compos Struct 2013;105:29–34.
[27] Madeira JFA, Araujo AL, Mota Soares CM, Mota Soares CA, Ferreira AJM. Multiobjective design of viscoelastic laminated composite sandwich panels. Compos B Eng 2015;77:391–401.
[28] Madeira JFA, Araujo AL, Mota Soares CM, Mota Soares CA [Multiobjective optimization of viscoelastic laminated sandwich structures using the Direct MultiSearch Method]. Comput Struct 2015;147:229–35.
[29] Franco Correia VM, Madeira JA, Araujo AL, Mota Soares CM [Multiobjective design optimization of laminated composite plates with piezoelectric layers]. Compos Struct 2017;169:10–20.
[30] Shen HS. Functionally graded material: nonlinear analysis of plates and shells. CRC Press; 2009.
[31] Shen HS, Wang ZX. Assessment of Voigt and Mori-Tanaka models for vibration analysis of functionally grades plates. Compos Struct 2012;94:2197–208.
[32] Reddy JN, Chin CD. Thermomechanical analysis of functionally graded cylinders and plates. J Therm Stress 1998;21:593–629.
[33] Javaheri R, Eslami MR. Thermal buckling of functionally graded plates. AIAA J 2002;40(1).
[34] Kar VR, Panda SK. Free vibration responses of temperature dependent functionally graded curved panels under thermal environment. Latin Am J Solids Struct 2015;12:2006–24.
[35] Reddy JN. Mechanics of laminated composite plates – theory and applications. CRC Press; 1997.
[36] Franco Correia VM, Gomes MA, Suleman A, Mota Soares CM, Mota Soares CA. Modelling and design of adaptive composite structures. Comput. Methods Appl. Mech. Eng. 2000;185:325–46.
[37] Franco Correia VM, Mota Soares CM, Mota Soares CA. Buckling optimization of composite laminated structures. Compos Struct 2003;62:315–21.
[38] Custodio AL, Madeira JFA. GLODS: global and local optimization using direct search. J Global Optim 2015;62(1):1–28.
[39] Miettinem K. Nonlinear multiobjective optimization. New York: Kluwer Academic Publishers; 1999.
[40] Kalyanmoy Deb K. Multiobjective optimization using evolutionary algorithms, J. Wiley & Sons; 2001.
[41] Zenkour A. Generalized shear deformation theory for bending analysis of functionally graded plates. Appl Math Model 2006;30:67–84.
[42] Thai HT, Choi DH. A simple first-order shear deformation theory for the bending and free vibration analysis of functionally graded plates. Compos Struct 2013;101:332–40.
[43] Bui TQ, Do TV, Ton LHT, Doan DH, Tanaka S, Pham DT, et al. On the high temperature mechanical behaviors analysis of heated functionally grade plates using FEM and a new third-order shear deformation theory. Compos B 2016;92:218–41.
[44] Qian LF, Batra RC, Chen LM. Static and dynamic deformations of thick functionally graded elastic plates by using higher-order shear and normal deformable plate theory and meshless local Petrov-Galerkin method. Compos B 2004;35:685–97.
[45] Neves AMA, Ferreira AJM, Carrera E, Roque CMC, Cinefra M, Jorge RMN. A quasi-3D sinusoidal shear deformation theory for the static and free vibration analysis of functionally graded plates. Compos Part B: Eng 2012;43(2):711–25.
[46] Neves AMA, Ferreira AJM, Carrera E, Cinefra M, Roque CMC, Jorge RMN. A quasi-3D hyperbolic shear deformation theory for the static and free vibration analysis of functionally graded plates. Compos Struct 2012;94(5):1814–25.
[47] Lafiti M, Farhatnia F, Kadkhodaei M. Buckling analysis of rectangular functionally graded plates under various edge conditions using Fourier series expansion. Eur J Mech A/Solids 2013;41:16–27.
[48] Thai HT, Choi DH. An efficient and simple refined theory for buckling analysis of functionally graded plates. Appl Math Model 2012;36:1008–22.
[49] Bodaghi M, Saidi AR. Levy-type solution for buckling analysis of thick functionally graded rectangular plates based on higher-order shear deformation plate theory. Appl Math Model 2010;34:3659–73.